Phosphorylation regulates targeting of cytoplasmic dynein to kinetochores during mitosis

Jacqueline Whyte,[1,2] Jason R. Bader,[1,2] Sinji B.F. Tauhata,[1,2] Maurice Raycroft,[1,2] Jessica Hornick,[1,2] K. Kevin Pfister,[3] William S. Lane,[4] Gordon K. Chan,[5] Edward H. Hinchcliffe,[1,2] Patricia S. Vaughan,[1,2] and Kevin T. Vaughan[1,2]

[1]Department of Biological Sciences and [2]Notre Dame Integrated Imaging Facility, University of Notre Dame, Notre Dame, IN 46556
[3]Department of Cell Biology, University of Virginia Health Sciences Center, Charlottesville, VA 22908
[4]Harvard Microchemistry and Proteomics Facility, Department of Molecular and Cellular Biology, Harvard University, Cambridge, MA 02138
[5]Department of Oncology, University of Alberta, Cross Cancer Institute, Edmonton, Alberta T6G1Z2, Canada

Cytoplasmic dynein functions at several sites during mitosis; however, the basis of targeting to each site remains unclear. Tandem mass spectrometry analysis of mitotic dynein revealed a phosphorylation site in the dynein intermediate chains (ICs) that mediates binding to kinetochores. IC phosphorylation directs binding to zw10 rather than dynactin, and this interaction is needed for kinetochore dynein localization. Phosphodynein associates with kinetochores from nuclear envelope breakdown to metaphase, but bioriented microtubule (MT) attachment and chromosome alignment induce IC dephosphorylation. IC dephosphorylation stimulates binding to dynactin and poleward streaming. MT depolymerization, release of kinetochore tension, and a PP1-γ mutant each inhibited IC dephosphorylation, leading to the retention of phosphodynein at kinetochores and reduced poleward streaming. The depletion of kinetochore dynactin by moderate levels of p50(dynamitin) expression disrupted the ability of dynein to remove checkpoint proteins by streaming at metaphase but not other aspects of kinetochore dynein activity. Together, these results suggest a new model for localization of kinetochore dynein and the contribution of kinetochore dynactin.

Introduction

Cytoplasmic dynein has been implicated in essential functions at the cell cortex, spindle poles, and kinetochores. The polar and cortical locations of dynein are consistent with roles in spindle assembly (Vaisberg et al., 1993; Gaglio et al., 1996; Heald et al., 1996; Merdes et al., 2000; Rusan et al., 2002) and spindle positioning (Li et al., 1993; Muhua et al., 1994; Carminati and Stearns, 1997; Adames and Cooper, 2000; O'Connell and Wang, 2000). In contrast, the functions of cytoplasmic dynein at kinetochores remain controversial (for reviews see McIntosh et al., 2002; Musacchio and Salmon, 2007). During prometaphase, dynein is thought to be part of a feedback mechanism that senses the degree of microtubule (MT) attachment (Wordeman et al., 1991; McEwen et al., 1998; Hoffman et al., 2001). Kinetochore dynein has also been implicated as a motor for chromosome move-

ment (Cande and Wolniak, 1978; Rieder and Alexander, 1990; Savoian et al., 2000; Sharp et al., 2000; Yang et al., 2007). Consistent with this function, localization studies place dynein on kinetochores primarily during prometaphase (Pfarr et al., 1990; Steuer et al., 1990; Wordeman et al., 1991; King et al., 2000), and dynein inhibition studies suggest a role in congression (Echeverri et al., 1996; Yang et al., 2007). Beyond metaphase, dynein has been implicated in anaphase chromosome movement (Sharp et al., 2000) and spindle elongation (for review see Banks and Heald, 2001). Together, these models support a role for dynein as a chromosome motor.

In addition to roles as a chromosome motor, dynein is thought to contribute to the spindle assembly checkpoint (SAC). As individual chromosomes approach the metaphase plate, multiple proteins release from kinetochores and stream toward the spindle poles (for review see Karess, 2005). One consequence of streaming is a reduction in the residence time of checkpoint

J. Whyte and J.R. Bader contributed equally to this paper.

Correspondence to Kevin T. Vaughan: Vaughan.4@nd.edu

Abbreviations used in this paper: ACA, autoimmune chromosomal antigen; CSF, cytostatic factor; IC, intermediate chain; IFM, immunofluorescence microscopy; LIC, light IC; MS, mass spectrometry; MT, microtubule; SAC, spindle assembly checkpoint; shRNA, short hairpin RNA.

The online version of this article contains supplemental material.

proteins at kinetochores, and this has been suggested as a mechanism to silence the SAC at metaphase. Dynein has been implicated as the motor for this streaming process (for reviews see Karess, 2005; Musacchio and Salmon, 2007), and inhibition of the dynein pathway affects streaming and the timing of anaphase onset (Howell et al., 2001; Wojcik et al., 2001; Basto et al., 2004).

Although roles as a chromosome motor or a motor for streaming of checkpoint proteins are not mutually exclusive, mechanisms to coordinate these functions or to activate dynein at the appropriate time are unknown. In this study, a new phosphorylation site was identified in the dynein intermediate chains (ICs) that is linked to the kinetochore localization of dynein. In the phosphorylated state, dynein is recruited to kinetochores through a direct interaction with *zw10*. After association with the mitotic spindle, dynein undergoes dephosphorylation coupled to dynein-driven streaming of checkpoint proteins. Because bioriented MT attachment and chromosome alignment induce this change in dynein activity, this work potentially provides insight into the molecular transitions needed for proper anaphase onset.

Results

Mitotic phosphorylation of cytoplasmic dynein ICs

Several studies suggest that cytoplasmic dynein is regulated by phosphorylation during mitosis (Niclas et al., 1996; Huang et al., 1999). Cytostatic factor (CSF)–arrested *Xenopus laevis* egg extracts contain phosphorylated cytoplasmic dynein (Niclas et al., 1996), and phospho-sensing antibodies label dynein subunits in these extracts (Huang et al., 1999). To better understand mitotic dynein phosphorylation in mammalian cells, individual subunits were analyzed for phosphorylation in dynein from synchronized HeLa cells (Fig. 1 A). A comparison of interphase and mitotic dynein subunits revealed a mitotic gel shift of the dynein ICs. Phosphatase treatment reversed the gel shift, confirming mitotic phosphorylation of the ICs. Analysis of a mitotic time course revealed conversion of the dynein ICs to primarily the gel-shifted form by 60 min after nocodazole washout (Fig. 1 B). Using a time point containing only the shifted form of the ICs, interphase and mitotic ICs were subjected to a blot overlay assay (Vaughan and Vallee, 1995; Vaughan et al., 2001; Deacon et al., 2003) to measure the impact on dynactin (p150^{Glued}) binding (Fig. 1 C). Similar to previous work, p150^{Glued} bound primarily to the dynein ICs in interphase extracts (Vaughan and Vallee, 1995). A comparison of interphase and mitotic samples revealed a significant reduction in binding of p150^{Glued} to mitotic ICs (Fig. 1 C). This suggests that mitotic dynein IC phosphorylation reduces binding to dynactin.

Mapping a novel phosphorylation site in mitotic dynein ICs

Because the domain structure of the dynein ICs is known (Vaughan and Vallee, 1995; Wilkerson et al., 1995; Lo et al., 2001; Mok et al., 2001; Susalka et al., 2002), phosphorylation sites implicated in regulating dynactin binding were expected near the N terminus (Vaughan et al., 2001). To test this prediction, the gel-shifted IC band was isolated from SDS-PAGE gels and sub-

jected to proteolytic digestion and tandem mass spectrometry (MS) electrospray analysis for evidence of protein phosphorylation. Collision-induced dissociation of proteolytic fragments revealed a novel phosphorylation site in the p150^{Glued}-binding domain of the ICs (T89; Fig. 1 D and Fig. S1, available at http://www.jcb.org/cgi/content/full/jcb.200804114/DC1). Phosphorylation at T89 appears to be a mitotic alternative to the interphase phosphorylation site mapped in previous work (S84; Vaughan et al., 2001). To test the effect of T89 phosphorylation, T89A/D/E mutants were prepared as recombinant proteins and compared for p150^{Glued}-binding activity using serial dilution slot blots. p150^{Glued} binding was not different for the T89A mutant (not depicted), but T89D/E mutants displayed an approximately four-fold reduction in binding (Fig. S1).

Phosphorylated dynein localizes to mitotic kinetochores

Cytoplasmic dynein is known to function at spindle poles (Gaglio et al., 1996; Heald et al., 1996), kinetochores (Pfarr et al., 1990; Steuer et al., 1990; Wordeman et al., 1991; Echeverri et al., 1996; Hoffman et al., 2001; Howell et al., 2001; Wojcik et al., 2001), and the cell cortex (Muhua et al., 1994; Carminati and Stearns, 1997; O'Connell and Wang, 2000; Dujardin and Vallee, 2002) during mitosis. Dynactin is thought to function with dynein at each of these sites (Dujardin and Vallee, 2002). Because phosphodynein displayed reduced binding to dynactin, the localization of phosphodynein was unclear. As an alternative to visualizing T89A/D/E mutants, which failed to function as effective localization probes, a new antibody was generated against a synthetic peptide containing phosphorylated T89 (PT89; Figs. S2 and S3, available at http://www.jcb.org/cgi/content/full/jcb.200804114/DC1). This PT89 antibody was used to determine the localization of phosphodynein in NRK2 cells (Fig. 2). In contrast to other dynein antibodies that label spindle poles, the cell cortex, and kinetochores, PT89-dynein localized primarily to kinetochores. Kinetochore labeling was evident from nuclear envelope breakdown to late prometaphase and was not detected on kinetochores after metaphase chromosome alignment. Because MT depolymerization induces exaggerated recruitment of dynein and other components to kinetochores (Wordeman et al., 1991), this approach was used to assess the impact on PT89-dynein. PT89-dynein displayed enhanced accumulation at kinetochores after nocodazole treatment and mirrored the overaccumulation of dynein observed with antibodies against total dynein. To confirm that the chromosome-associated accumulations of PT89-dynein corresponded to kinetochores, PT89-dynein localization was compared with the autoimmune chromosomal antigen (ACA; not depicted) and BubR1 (Fig. 2). PT89-dynein colocalized with both markers; however, BubR1 was a more reliable marker for colocalization experiments in NRK2 cells.

The levels of PT89-dynein at kinetochores underwent an intriguing change as chromosomes became associated with mitotic spindles, proceeded through congression, and aligned at the metaphase plate. PT89-dynein labeling was most intense on kinetochores with no MT attachments or monooriented attachments (Fig. 2). After association with the mitotic spindle, PT89-dynein levels displayed a gradual reduction that correlated with
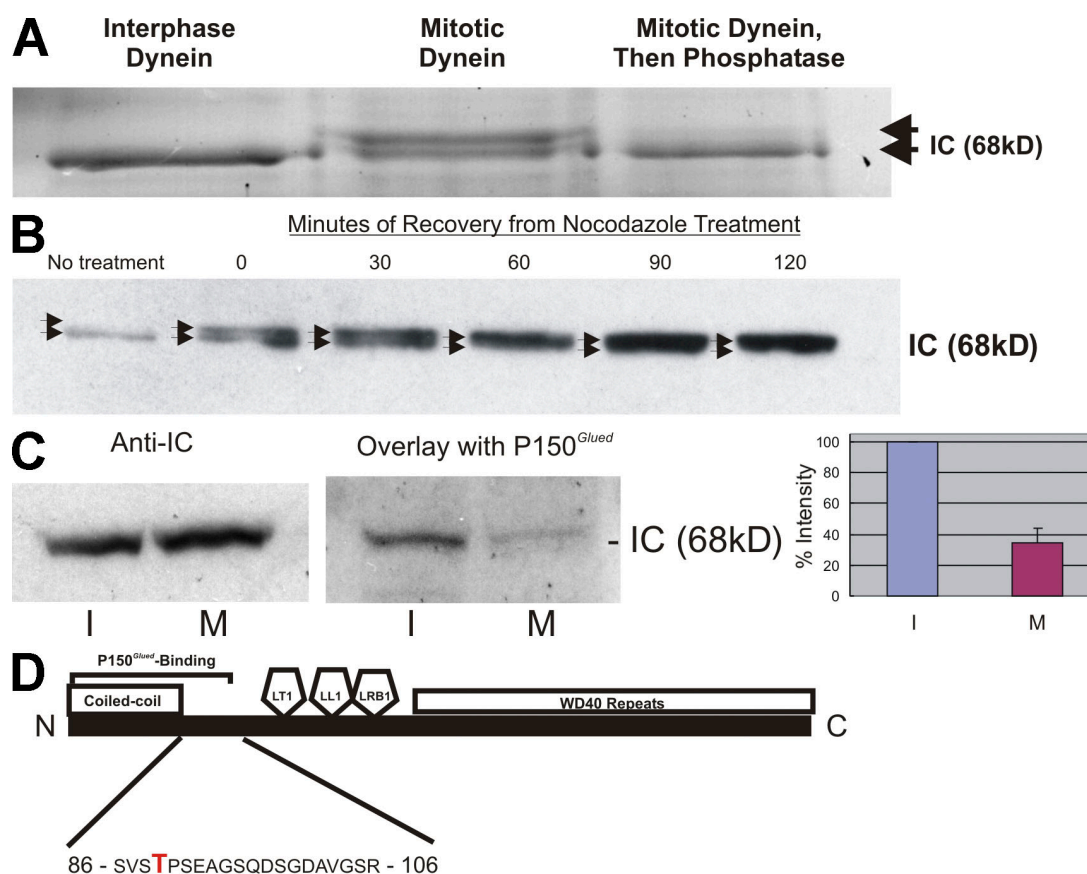
Figure 1. **Mitotic phosphorylation of the cytoplasmic dynein ICs.** (A) SDS-PAGE analysis of HeLa cell cytoplasmic dynein. Dynein ICs (arrows) displayed a gel shift in mitotic but not interphase samples, and the gel-shifted form was eliminated by λ-phosphatase treatment. (B) Western blot analysis of dynein ICs at time points after nocodazole washout. Arrows indicate two variants of the dynein ICs. (C) Blot overlay analysis of interphase and mitotic ICs using recombinant p150[Glued]. Controls confirm equivalent loading of interphase (I) and mitotic (M) dynein ICs. Overlay assays reveal reduced binding to mitotic ICs compared with interphase ICs. The signal of the interphase sample was scored as 100%, and the signal of the mitotic sample was measured as a percentage of the interphase sample after background subtraction ($n = 3$; $P = 0.007$). Error bar represents SD. (D) Gel-shifted IC gel bands were subjected to in-gel tryptic/chymotryptic digestion and microcapillary liquid chromatography tandem MS analysis. Collision-induced dissociation identified the phosphorylated residue as T89 (Fig. S1 A, available at http://www.jcb.org/cgi/content/full/jcb.200804114/DC1).

bioriented MT attachment and chromosome alignment. The PT89 signal was largely lost on kinetochores that were aligned at the metaphase plate (Fig. 2) and was not observed on kinetochores after anaphase onset.

Although specific antibodies against the dephospho form of dynein were not available, a comparison of PT89-dynein with total dynein was possible. The reduction in PT89-dynein signal observed from prometaphase to metaphase was coupled with enhanced labeling for total dynein along kinetochore MT fibers and at spindle poles (Fig. 2). Interestingly, PT89-dynein labeling was observed at kinetochores but not along kinetochore fibers or spindle poles. At metaphase, when PT89-dynein labeling at kinetochores was weakest, total dynein was observed along kinetochore fibers and at spindle poles but not at kinetochores. One possibility suggested by these observations is that kinetochore dynein is converted from a phosphorylated to dephosphorylated state during chromosome alignment and that this transition stimulates poleward movement of dynein. Because dephosphodynein binds to dynactin, this would be consistent with the streaming of a dynein–dynactin complex suggested by previous work (Howell et al., 2001; Wojcik et al., 2001; Basto et al., 2004).

Recruitment of phosphorylated dynein to kinetochores independent of dynactin

The localization of PT89-dynein to kinetochores was unexpected given existing models for dynein targeting. Previous work implicates the dynactin complex in the recruitment of cytoplasmic dynein to kinetochores (Echeverri et al., 1996; Howell et al., 2001; Wojcik et al., 2001; Basto et al., 2004), and PT89-dynein displays reduced affinity for p150[Glued]/dynactin (Fig. 1). To test whether dynactin was required for recruitment of PT89-dynein, p50(dynamitin) overexpression was used to reduce dynactin at kinetochores (Echeverri et al., 1996). To allow imaging of cells expressing low to moderate amounts of p50(dynamitin), a new construct expressing mCherry-p50(dynamitin) was generated. Using antibodies against dynactin and tubulin to screen transfected cells, three distinct phenotypes were observed, reflecting the relative levels of p50(dynamitin) expression. Cells expressing the lowest levels of p50(dynamitin) displayed no obvious disruption phenotypes (Fig. 3, A and B), and the transfected protein marked kinetochores and spindle poles throughout prometaphase (see Fig. 7 B). Cells expressing intermediate levels of p50(dynamitin) displayed substantial depletion of p150[Glued] at kinetochores but assembled and maintained relatively normal mitotic
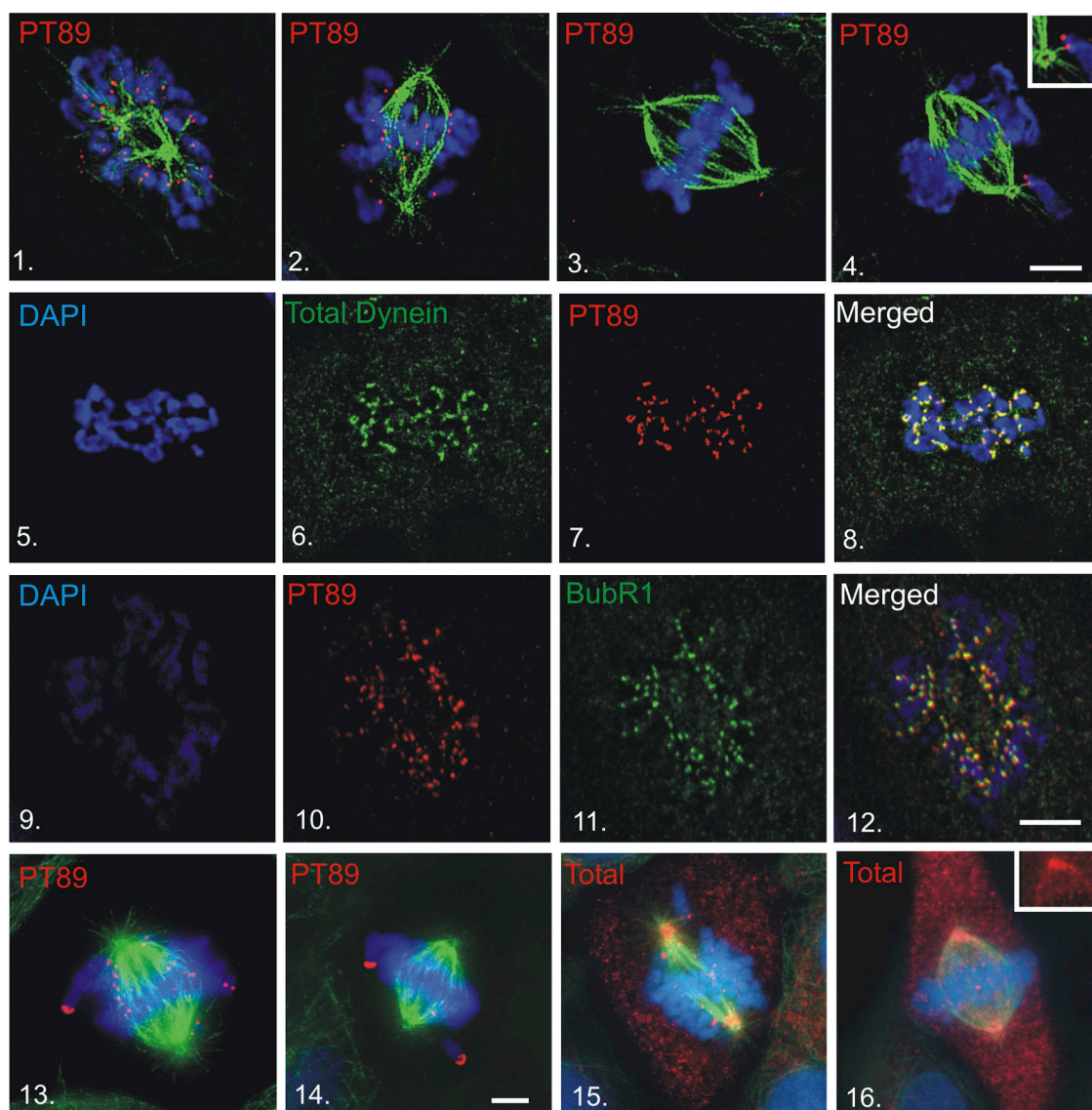
Figure 2. **Mitotic localization of phosphorylated dynein.** (1–4) NRK2 cells stained for chromatin (DAPI, blue), tubulin (green), and PT89-dynein (red) reveal PT89 at kinetochores at early prometaphase (1), late prometaphase (2), and on kinetochores of monooriented chromosomes (4). PT89-dynein is absent on kinetochores of aligned chromosomes at metaphase (3). The inset in panel 4 shows the image at a higher magnification. (5–8) Nocodazole-treated NRK2 cells were stained for chromatin (5 and 8), 74.1 antibody against the dynein ICs (6 and 8; Dillman et al., 1996), and PT89-dynein (7 and 8). Merged image confirms colocalization on kinetochores (8). (9–12) NRK2 cells stained for chromatin (9), PT89-dynein (10), and BubR1 (11) reveal colocalization of PT89-dynein with BubR1. (13–16) NRK2 cells stained for chromatin (DAPI, blue), tubulin (green), and PT89-dynein (13 and 14) reveal that the PT89-dynein signal is prominent on kinetochores of unaligned chromosomes but reduced on kinetochores close to the metaphase plate. V3 (against total dynein ICs; 15 and 16) is prominent on kinetochores during prometaphase but weaker along spindle fibers and spindle poles. In contrast, the V3 signal is weak on aligned kinetochores at metaphase but prominent along spindle fibers and at spindle poles (16, inset). Bars, 5 µm.

spindles without congression defects (Fig. 3 and Fig. S4, available at http://www.jcb.org/cgi/content/full/jcb.200804114/DC1). Cells expressing the highest levels of p50(dynamitin) displayed the wide range of spindle defects observed by others (Echeverri et al., 1996), including splayed spindle poles and congression errors (Fig. 3, A and B).

To characterize the impact of moderate levels of p50(dynamitin) expression on mitotic progression, live cell imaging was performed on cells coexpressing GFP–histone 2B (H2B). Control cells displayed normal chromosome alignment and spent ~8 min at metaphase before anaphase onset (Fig. 3 C, Fig. S4, and Video 1, available at http://www.jcb.org/cgi/content/

full/jcb.200804114/DC1). Cells expressing moderate levels of p50(dynamitin) also aligned chromosomes at the metaphase plate with normal kinetics. The most obvious phenotype observed in these p50(dynamitin)-expressing cells was metaphase arrest or delay where the mean time spent at metaphase increased to >30 min (Fig. 3 C, Fig. S4, and Video 2). These experiments indicate that moderate expression of mCherry-p50(dynamitin) is effective at reducing levels of dynactin at kinetochores without other major spindle problems and that the phenotype induced by this dynactin depletion is metaphase arrest/delay.

Having assessed the effects of moderate p50(dynamitin) expression, we tested the impact on recruitment of dynein to
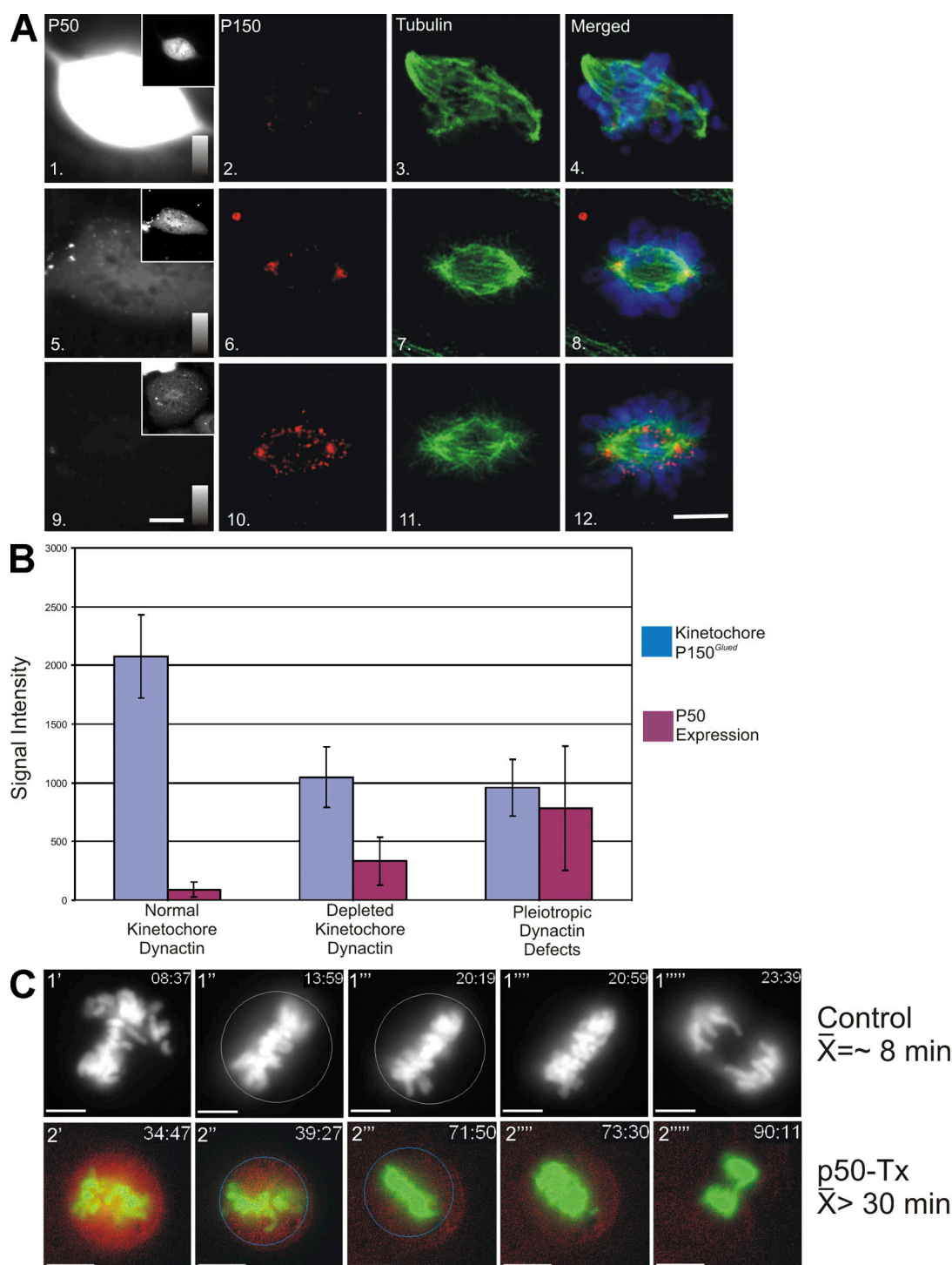
Figure 3. **Impact of p50(dynamitin) expression on kinetochore dynactin and spindle integrity.** (A) NRK2 cells expressing high (panels 1–4), moderate (panels 5–8), and low (panels 9–12) levels of mCherry-tagged p50(dynamitin) (panels 1, 5, and 9) were stained for p150^{Glued} (panels 2, 6, and 10) and tubulin (panels 3, 7, and 11). Images of p50(dynamitin) levels are scaled the same in panels 1, 5, and 9 and can be compared using the intensity scales in each panel. The insets in panels 1, 5, and 9 demonstrate transfection of each example and the distribution of the transfected protein. These cells ($n = 89$) were used to correlate expression levels with mitotic defects. (B) Transfectants were binned into three categories based on level of expression: (1) low levels of expression (mean = 99, $n = 31$), which displayed no defects in kinetochore dynactin or spindle formation; (2) moderate levels of expression (mean = 381, $n = 27$), which displayed loss of kinetochore dynactin but normal spindle function; and (3) high levels of expression (mean = 980, $n = 31$), which displayed pleiotropic defects in spindle function and loss of kinetochore dynactin. Error bars represent SD. (C) NRK2 cells expressing GFP-H2B were subjected to time-lapse imaging. In controls (1′–1′′′′′), time-lapse sequences were used to determine the point of chromosome alignment, and the chromosome mass was circled (1′′). The timing of anaphase onset is indicated by deletion of the circle (1′′′′), and the time between these points was recorded. The mean time for controls (8.055 ± 3.01 min; $n = 10$) differed from cells transfected with mCherry-tagged p50(dynamitin) (p50-Tx; 2′–2′′′′′) cells that initiated anaphase a mean of 17.60 ± 7.9 min after alignment ($n = 10$). Another population of p50-transfected cells never entered anaphase within the time frame of imaging ($n = 7$), and the mean (51.31 ± 24.66 min) reflects the timing until imaging was terminated (Fig. S4 and Videos 1–4, available at http://www.jcb.org/cgi/content/full/jcb.200804114/DC1). Bars, 5 μm.
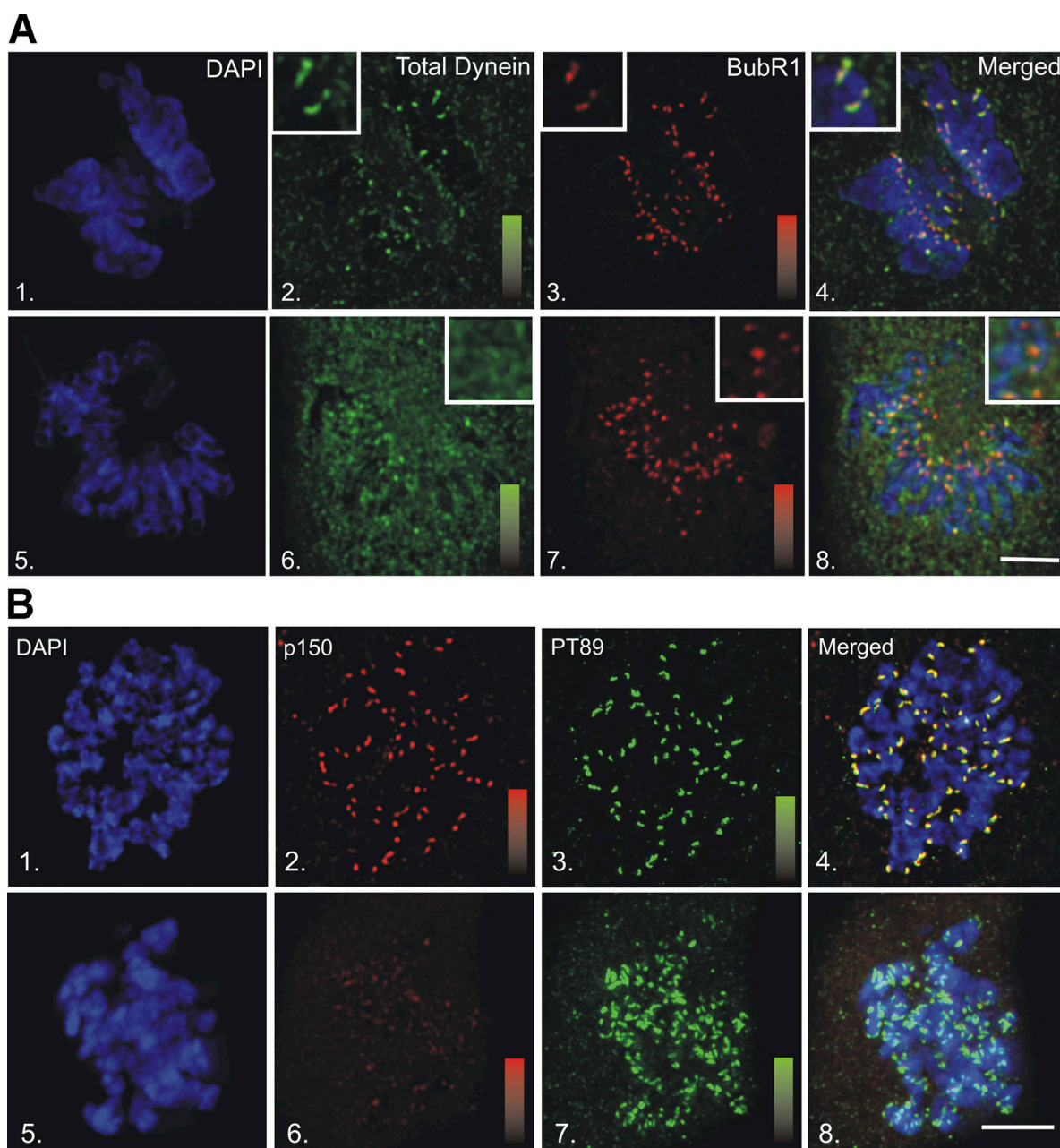
Figure 4. **Impact of p50(dynamitin) expression on PT89-dynein localization.** (A) Control (1–4) and p50(dynamitin)-expressing (5–8) NRK2 cells stained for chromatin (DAPI; 1 and 5), total dynein ICs (V3; 2 and 6), and BubR1 (3 and 7) reveal a colocalization of total dynein with BubR1 on kinetochores during prometaphase in controls (4, inset) but a depletion of total dynein from prometaphase kinetochores in cells expressing moderate levels of p50(dynamitin) (8, inset). Intensity scales in panels 2 and 6 correspond to levels from 0 to 800 intensity units. (B) Nocodazole-treated control (1–4) and p50(dynamitin)-expressing (5–8) NRK2 cells stained for chromatin (DAPI; 1 and 5), p150^{Glued} (2 and 6), and PT89-dynein (3 and 7) reveal similar levels of PT89-dynein on kinetochores with normal (2 and 4) or depleted (6 and 8) levels of p150^{Glued}. Bars, 5 µm.

kinetochores. To compare our results with previous work (Echeverri et al., 1996), we compared control and p50(dynamitin)-expressing cells for effects on the levels of total dynein (Fig. 4 A). Similar to previous studies, moderate expression of the new mCherry-tagged p50(dynamitin) construct resulted in a reduction in levels of dynactin (Fig. 4 B and Fig. S4) and total dynein at kinetochores (Fig. 4 A) and correlated with a greater soluble pool of dynein (Fig. 4 A; Echeverri et al., 1996). In contrast, when cells depleted of kinetochore dynactin were assessed for effects on phosphodynein, levels of PT89-dynein at these kinetochores

were normal. The effect on PT89 staining was most obvious in nocodazole-treated cells where phosphodynein levels on each kinetochore were the same (Fig. 4 B and Fig. S4). This suggests that the binding of PT89-dynein to kinetochores is not dependent on kinetochore dynactin.

A novel binding partner for phosphodynein

The dynactin-independent binding of PT89-dynein to kinetochores implicated a new binding partner in recruiting dynein to kinetochores. Several proteins have been linked to dynein

levels at kinetochores recently, including LIS-1 (Faulkner et al., 2000), *nudE/EL* (Stehman et al., 2007; Vergnolle and Taylor, 2007), *nudC* (Zhou et al., 2006), *spindly* (Griffis et al., 2007), and *zw10* (Kops et al., 2005). With this list of potential candidates in mind, protein–protein interaction assays were performed comparing the binding of phospho- and dephosphodynein ICs with total extracts. Recombinant IC-2C was used as the dephosphorylated ICs, and this protein was subjected to in vitro phosphorylation reactions to generate the phosphorylated form of the ICs (Fig. S2). Consistent with previous work, dephosphorylated IC-2C displayed binding to the p150^{Glued} subunit of dynactin (Fig. 5 A; Vaughan et al., 2001). In contrast, phospho-ICs displayed reduced binding to p150^{Glued} and enhanced binding to a new protein band with an M_r of ~90 kD (Fig. 5 A). Because endogenous dynein ICs are detected as part of the assay and provide an internal standard (Vaughan and Vallee, 1995), the degree of differential binding was quantified between phospho- and dephospho-ICs. Phospho-ICs displayed an ~45% decrease in binding to p150^{Glued} (Fig. 5 A). The reduced binding to p150^{Glued} was coupled with a threefold increase in binding of phospho-IC to the 90-kD protein (Fig. 5 A). These results suggest that IC phosphorylation couples reduced p150^{Glued} binding with enhanced affinity for a new binding partner.

Growing evidence that the *rod–zw10–zwilch* complex is linked to dynein and dynactin at the kinetochore suggested a candidate for the 90-kD protein (Starr et al., 1998; Williams et al., 2003; Kops et al., 2005). Western blots performed in parallel with the overlays revealed that the 90-kD band co-migrated with *zw10* (Fig. 5 A) but not *rod* or *zwilch* (not depicted). To confirm the identification of *zw10*, an existing antibody (Chan et al., 2000) was used to immunoprecipitate *zw10* from mitotic extracts, and overlay assays were repeated with phospho-ICs. Phospho-IC bound to the *zw10* band in this sample (Fig. 5 A). A direct comparison of the wild-type and T89A/D mutant ICs revealed that dephospho-IC and T89A and T89D ICs displayed similar binding affinity for *zw10*, whereas phospho-ICs displayed approximately double the affinity for *zw10* (Fig. 5 B). This suggests that although the T89D/E mutations reduce the affinity of ICs for p150^{Glued}, they do not fully recapitulate the phospho-specific binding to *zw10*.

Additional evidence for an interaction between *zw10* and phospho-IC was obtained through short hairpin RNA (shRNA)–based depletion of *zw10* (Fig. 5 C). *zw10*-directed shRNA plasmids were effective at reducing the levels of *zw10* in NRK2 cells (Fig. 5 C), and this reduction also led to a substantial decrease in PT89 labeling of mitotic kinetochores (Fig. 5 D). This decrease in PT89-dynein was paralleled by a loss of total dynein at kinetochores during prometaphase (unpublished data). These results implicate a direct interaction between phospho-dynein and *zw10* as the basis of initial dynein recruitment to kinetochores. They also implicate the IC phosphorylation state as the basis of differential interactions with *zw10* and p150^{Glued}. In addition, because *zw10* appears to associate primarily with kinetochores, a specific interaction between phosphodynein and *zw10* provides a potential mechanism for targeting dynein to kinetochores.

Cytoplasmic dynein dephosphorylation is stimulated by MT attachment and tension

Although these experiments suggest that dynein is initially targeted to kinetochores in the phosphorylated state, dynein undergoes dephosphorylation that is linked to chromosome alignment (Fig. 2). To determine the requirements for loss of PT89-dynein at kinetochores, MT attachment and tension were examined. To test the role of MT attachment, untreated and nocodazole-treated cells were compared for effects on PT89-dynein. In untreated cells, both PT89 and the checkpoint protein BubR1 were lost from kinetochores by the time of metaphase chromosome alignment (Fig. 6 A). This is consistent with work on other checkpoint markers such as *mad2* (Howell et al., 2000), *rod* (Wojcik et al., 2001; Basto et al., 2004), and *zw10* (Basto et al., 2004; Kops et al., 2005). In contrast, the depolymerization of MTs with nocodazole (Fig. 6 A) resulted in the retention of both PT89 and BubR1 signals at kinetochores even in cells that have accomplished chromosome alignment. Measurement of interkinetochore distances confirmed a relaxed state in these kinetochores, which is consistent with a lack of MT attachment (Fig. S4). This suggests that dephosphorylation of PT89 requires MT attachment.

The contributions of MT attachment and kinetochore tension in the SAC are still under investigation (Nicklas et al., 1995; Waters et al., 1998; King et al., 2000; Shannon et al., 2002; Pinsky and Biggins, 2005), so the importance of tension was tested using brief treatment with taxol. This approach maintains MT attachment but reduces tension at the kinetochores of aligned chromosomes (Waters et al., 1998). Interkinetochore distance measurements confirmed decreased tension but not the completely relaxed kinetochore state observed in nocodazole (Fig. S4). PT89 signal was retained at the kinetochores of taxol-treated cells (Fig. 6 A) at levels similar to nocodazole-treated cells. As in nocodazole-treated cells, the retention of PT89 was linked to the retention of BubR1. Together, these results suggest that effective dynein dephosphorylation requires both MT attachment and kinetochore tension.

The requirement for both MT attachment and tension was reminiscent of previous work on kinetochore phosphoproteins. Some of these phosphoproteins are thought to be substrates for an unknown "tension-sensing" phosphatase that is coupled to the SAC (Gorbsky and Ricketts, 1993; Nicklas et al., 1995). To determine the impact of inhibiting dynein dephosphorylation, cells were treated with low levels of the phosphatase inhibitor calyculin A. This cell-permeable drug inhibits both PP1 and PP2 (protein phosphatases 1 and 2, respectively), overlaps with drugs used previously (i.e., microcystin), but can be used to treat living cells. Calyculin A treatment resulted in the retention of PT89 signal at kinetochores (Fig. 6 A) despite the completion of chromosome alignment and strong kinetochore tension as indicated by kinetochore stretch (Fig. S4). In addition, BubR1 was retained on kinetochores with PT89 (Fig. 6 A). Together, these experiments reveal that the loss of PT89-dynein signal at metaphase requires MT attachment, interkinetochore tension, and a calyculin A–sensitive phosphatase pathway. Each of these activities could contribute to the mechanisms that sense chromosome alignment at metaphase.
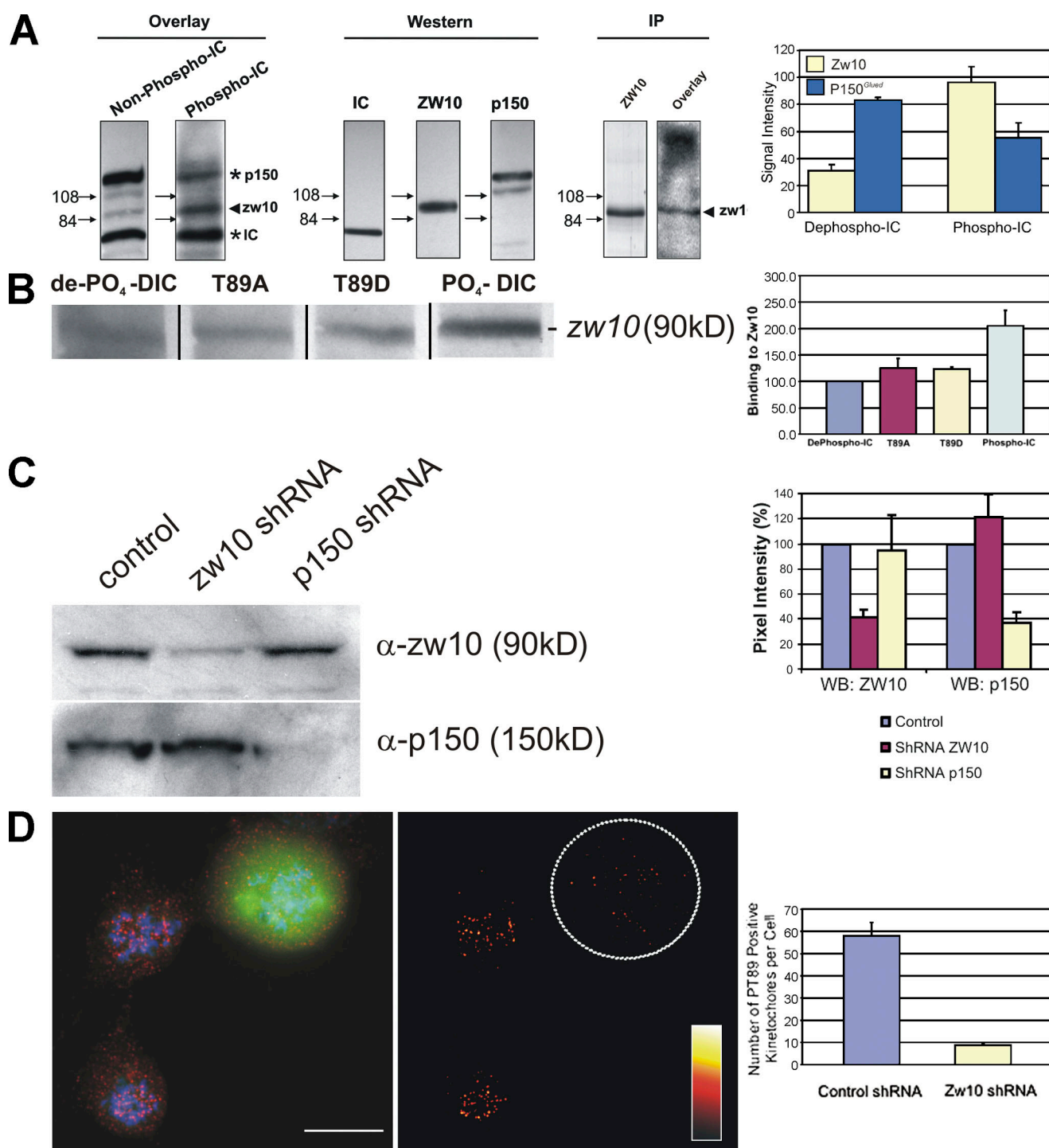
Figure 5.   **Differential binding of phosphodynein and dephosphodynein.** (A) Blot overlay assays demonstrate binding of dephospho-ICs to p150*Glued* but reduced binding of phospho-ICs to p150*Glued* coupled with enhanced binding to an ~90-kD protein that co-migrates with *zw10*. Blot overlays of *zw10* immunoprecipitates with phospho-ICs display this interaction in parallel. The binding of ICs to p150*Glued* changes from an intensity of 83.02% of ICs to 55.39% of ICs after phosphorylation (P = 0.0111), whereas binding of ICs to *zw10* increases from 31.12% of ICs to 96.22% of ICs after IC phosphoryla-tion (P = 0.0004). The numbers to the left of the blots indicate the measurement in kilodaltons. (B) Binding of dephospho-ICs (de-PO$_4$-DIC), T89A and T89D mutant ICs, and phospho-ICs (PO$_4$-DIC) to *zw10* revealed enhanced binding for only phospho-ICs (~100% increase). Differences between T89A/T89D mutants and the dephospho-ICs were not significant, whereas the difference between dephospho- and phospho-ICs was significant (P = 0.012). Black lines indicate that intervening lanes have been spliced out. (C) Western blot (WB) analysis demonstrating shRNA-based differences. shRNA-based depletion of *zw10* and p150*Glued* revealed an ~60% decrease in *zw10* signal after *zw10* depletion but no effect on p150*Glued*. shRNA-based depletion of p150*Glued* resulted in depletion of p150*Glued* but had no effect on *zw10*. (D) IFM analysis of PT89-dynein in mitotic cells revealed loss of PT89 signal (red) in cells treated with *zw10* shRNA constructs encoding GFP. PT89 signal intensity is presented using a color gradient representing intensities of 0–2,300 intensity units. The number of kinetochores displaying control mean intensity are compared for control and *zw10*-depleted cells (P < 0.05). The circled area shows a cell expressing *zw10* shRNA. Error bars represent SD. Bar, 5 µm.
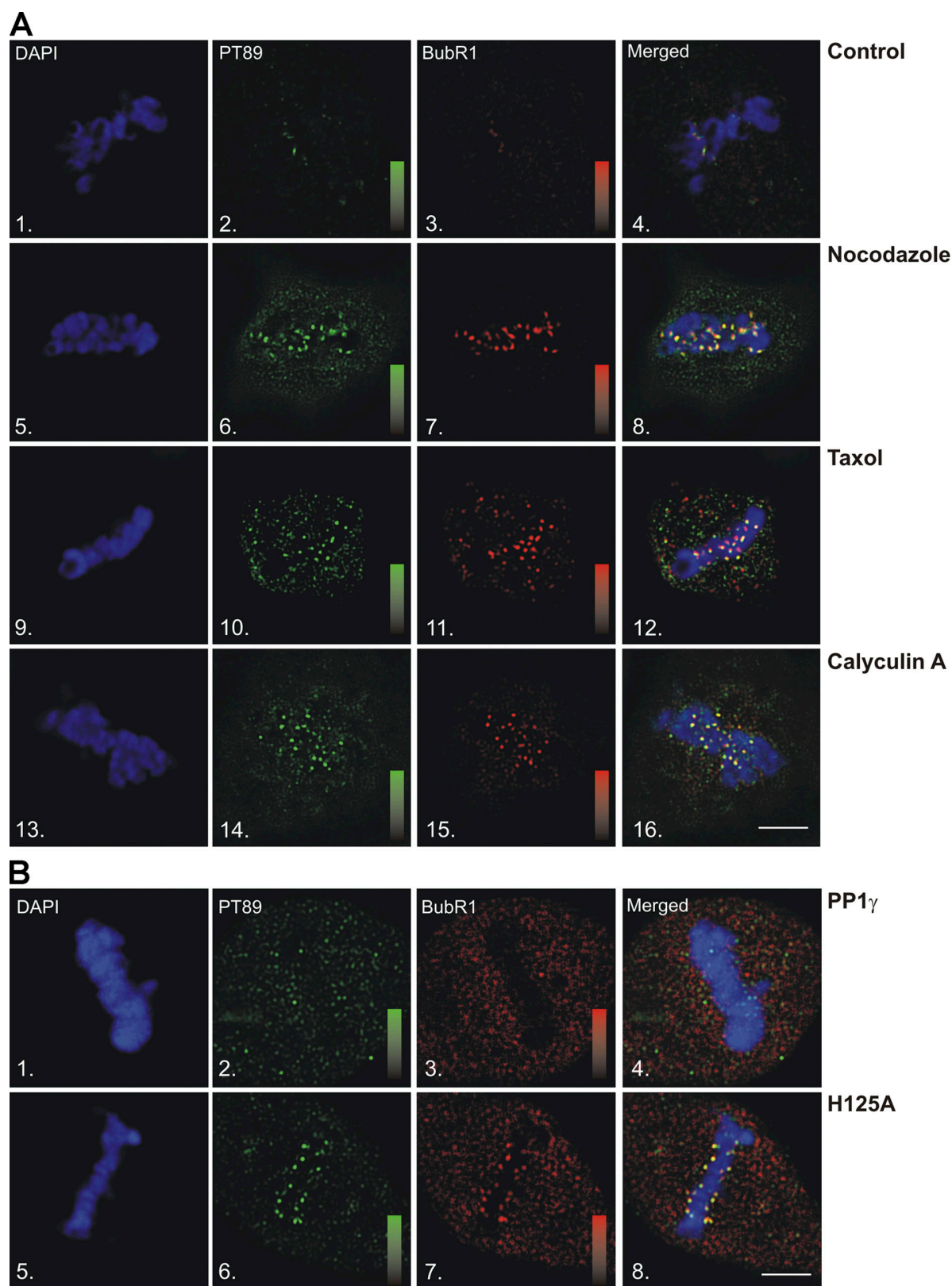
Figure 6. **Dynein dephosphorylation requires MT attachment and tension.** (A) IFM analysis of methanol-fixed NRK2 cells stained for chromosomes (DAPI; 1, 5, 9, and 13), phosphodynein (PT89; 2, 6, 10, and 14), and BubR1 (3, 7, 11, and 15) was performed after the following treatments: untreated (1–4), nocodazole (5–8), taxol (9–12), and calyculin A (13–16). Methanol fixation preserves kinetochore- but not spindle-associated BubR1. (B) NRK2 cells were transfected with GFP-tagged wild-type (1–4) or YFP-tagged H125A mutant PP1-γ (5–8) and stained for chromosomes (1 and 5), PT89 (2 and 6), or BubR1 (3 and 7). (A and B) Scales display fluorescence intensity ranges of 1–1,000 intensity units for PT89 and 0–1,200 intensity units for BubR1. Bars, 5 μm.

The results of calyculin A treatment and previous work on PP1 (Trinkle-Mulcahy et al., 2003) suggested PP1-γ as a potential dynein phosphatase. Wild-type and a phosphatase-dead H125A mutant PP1-γ (Lesage et al., 2004) were transfected into NRK2 cells, and PT89 signal on aligned chromosomes was measured. Consistent with previous work (Trinkle-Mulcahy et al., 2003), PP1-γ localized to kinetochores in live cell imaging (unpublished data). Cells transfected with wild-type PP1-γ displayed no defects in PT89 signal and shed both PT89 and BubR1 signal by the time of metaphase alignment as normal (Fig. 6 B). In contrast, cells transfected with the H125A mutant PP1-γ displayed retention of PT89 and BubR1 despite the completion of chromosome alignment (Fig. 6 B). Interkinetochore distance measurements revealed the highest degree of stretch in this experiment (Fig. S4). The levels of PT89 were also slightly higher than that of calyculin A–treated cells, suggesting a more complete inhibition of dynein dephosphorylation than the drug treatment. Together, these results link dynein dephosphorylation to progression through chromosome alignment and suggest that the degree of dynein dephosphorylation is controlled by PP1-γ, which could be stimulated at metaphase.

Dynein streaming is perturbed by inhibition of dynein dephosphorylation

The differential localization of phosphodynein at kinetochores and dephosphodynein along spindle fibers suggested that some spindle-associated dynein is translocating from kinetochores to spindle poles. To test this relationship, dynein dephosphorylation was blocked with brief taxol treatment, and the levels of dephosphodynein along spindle fibers were measured. In control cells, dynein was largely absent from kinetochores by metaphase but prominent along spindle fibers and at spindle poles (Fig. 7 A). After taxol treatment (Fig. 6), dynein remained detectable at kinetochores and was less prominent along spindle fibers and at spindle poles (Fig. 7 A). This suggests that some spindle fiber–associated dynein reflects dynein streaming from kinetochores to spindle poles and that dynein streaming requires IC dephosphorylation.

Because dynein is also implicated in spindle pole focusing and MT sliding, we used live cell imaging to test whether spindle-associated dynein emanated from kinetochores and whether this was sensitive to taxol treatment. p50(dynamitin) was an effective marker of kinetochores but not disruptive under conditions of very low expression (Fig. 3), so we performed live cell imaging in cells expressing low levels of GFP-p50(dynamitin) (Fig. 7, B and C). In control cells analyzed at metaphase, GFP-p50(dynamitin) displayed poleward movement along kinetochore fibers at rates of ∼1.3 μm/s, which is consistent with dynein-driven streaming (Fig. 7 B and Video 3, available at http://www.jcb.org/cgi/content/full/jcb.200804114/DC1). Coupled with this motility, the signal levels of GFP-p50(dynamitin) at kinetochores dropped progressively, suggesting depletion of kinetochore proteins by streaming (Fig. 7 C). Taxol treatment had a dramatic impact on this activity and blocked the poleward movement of p50(dynamitin) at metaphase (Fig. 7 B and Video 4). Coupled with this, GFP-p50(dynamitin) signal at kinetochores did not undergo the progressive depletion observed in controls (Fig. 7 C). This suggests that the spindle-associated population

of dynein observed at metaphase reflects the streaming process implicated in silencing the SAC.

Contributions of dynactin at kinetochores

Previous work had suggested that dynactin was required for the localization of dynein to kinetochores (Echeverri et al., 1996). Although this study suggests that dynactin is not required for initial recruitment of PT89-dynein to kinetochores, dynactin affects the levels of total dynein at kinetochores and plays an important role in dynein activity (Echeverri et al., 1996; Howell et al., 2001; Wojcik et al., 2001; Basto et al., 2004). Because moderate expression of p50(dynamitin) reduced the levels of dynactin at kinetochores without affecting the mitotic spindle globally, we focused on this approach to dissect the roles of kinetochore dynactin. Based on previous work (Echeverri et al., 1996; Howell et al., 2001; Wojcik et al., 2001; Basto et al., 2004), loss of kinetochore dynactin could (1) inhibit dynein dephosphorylation, (2) inactivate poleward dynein motility, or (3) uncouple dynein from kinetochore-specific cargoes. To assess these possibilities, cells were analyzed for localization of PT89-dynein, total dynein, and checkpoint proteins at metaphase. To measure the impact on PT89 dephosphorylation, control and p50(dynamitin)-expressing cells were compared for loss of PT89 signal at metaphase (Fig. 8 A). PT89 signal was lost at metaphase kinetochores under both conditions, suggesting that kinetochore dynactin is not required for dynein dephosphorylation at metaphase (Fig. 8 A). To measure the impact on poleward motility of the dynein complex, control and p50(dynamitin)-expressing cells were stained for total dynein and the checkpoint protein BubR1 (Fig. 8 B). In control cells, total dynein localization shifted comprehensively from kinetochores to spindle fibers and poles by the time of chromosome alignment (Fig. 8 B). This streaming was mirrored by BubR1, which no longer localized to kinetochores but rather labeled spindle fibers and poles in controls (Fig. 8 B). In p50(dynamitin)-expressing cells, total dynein labeling shifted from kinetochores to spindle fibers and poles as normal (Fig. 8 B). This suggests that the dynein complex can release from kinetochores and stream in the absence of dynactin. In contrast, the localization of BubR1 was strikingly different in p50(dynamitin)-transfected cells (Fig. 8 B). Despite the shift of dynein from kinetochores to spindle fibers and poles (Fig. 8 B), BubR1 continued to concentrate on kinetochores and failed to colocalize with dynein along spindle fibers (Fig. 8 B). Consistent with previous work, this result suggests that dynactin is required to couple streaming dynein to kinetochore-bound checkpoint proteins at metaphase (Howell et al., 2001; Wojcik et al., 2001; Basto et al., 2004). However, other aspects of dynein function are not affected dramatically after p50(dynamitin) expression, including initial recruitment to kinetochores, dynein dephosphorylation, or poleward motility of the dynein holoenzyme.

Discussion

The mapping of a novel phosphorylation site in the cytoplasmic dynein ICs reveals that two forms of dynein exist at kinetochores interacting with different binding partners. The phosphorylated form is recruited to kinetochores and interacts with the mitotic checkpoint protein *zw10*. The dephosphorylated form interacts
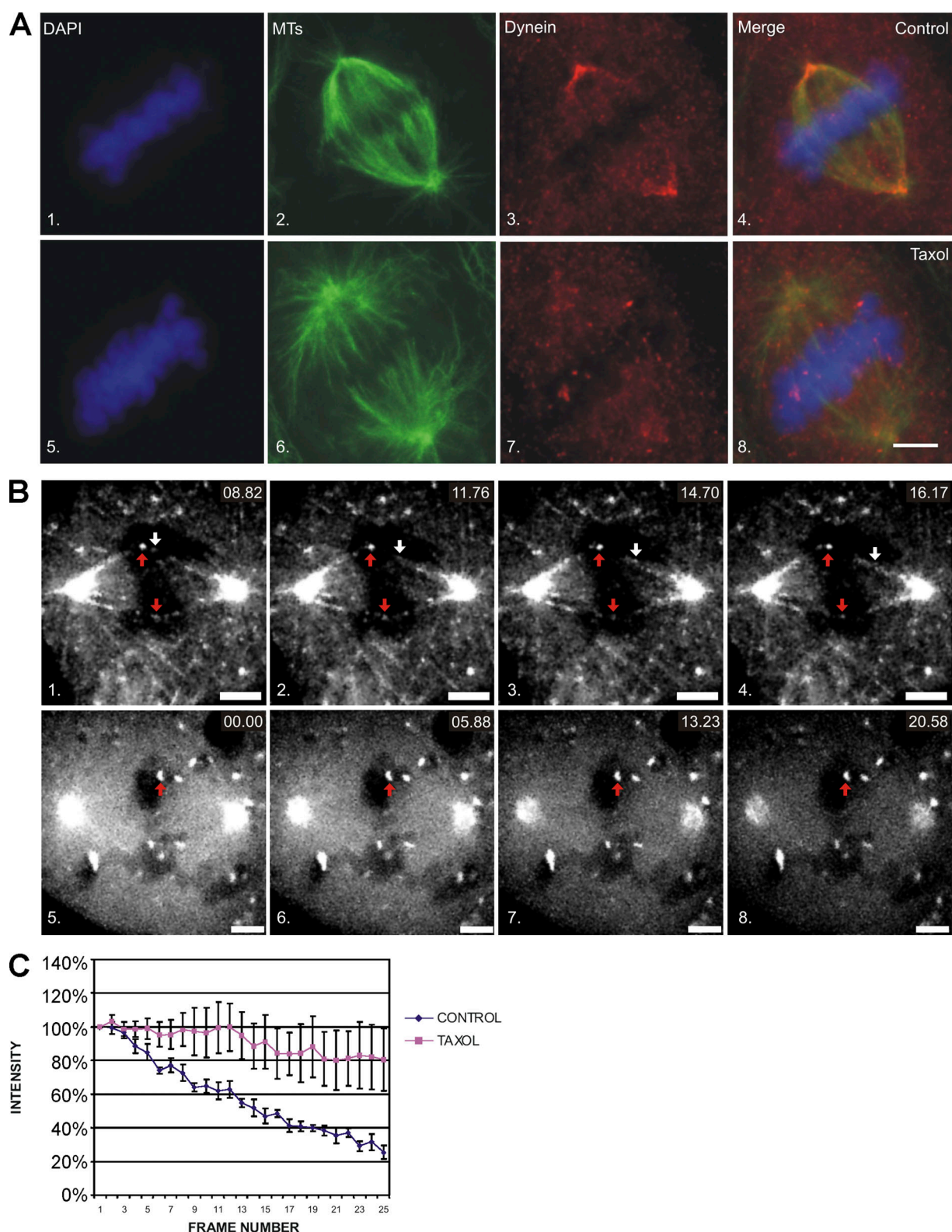
Figure 7.   **Inhibition of dynein dephosphorylation reduces poleward streaming of dynein.** (A) NRK2 cells stained for DAPI (1 and 5), tubulin (2 and 6), and total dynein (3 and 7) at metaphase reveal a loss of the PT89 signal at kinetochores, but it is present at spindle poles and along spindle fibers in controls (1–4). Dynein is still detected at kinetochores but is less prominent at spindle poles and along spindle fibers in cells treated with taxol (5–8). (B) Live cell analysis of metaphase cells expressing low levels of GFP-p50(dynamitin) under control conditions (1–4) or after treatment with taxol (5–8). Particles of GFP-p50(dynamitin) labeling (white arrows) can be seen moving poleward from kinetochores (red arrows) and label spindle fibers in controls (1–4; Video 3, available at http://www.jcb.org/cgi/content/full/jcb.200804114/DC1). After taxol treatment (5–8; Video 4), GFP-p50(dynamitin) labeling is intense at kinetochores but does not exhibit movement or label spindle fibers. (C) Line plot of GFP-p50(dynamitin) intensities for control and taxol-treated cells. Intensity measurements were collected for five kinetochores, and mean intensity is plotted with SD (error bars). Bars, 5 µm.
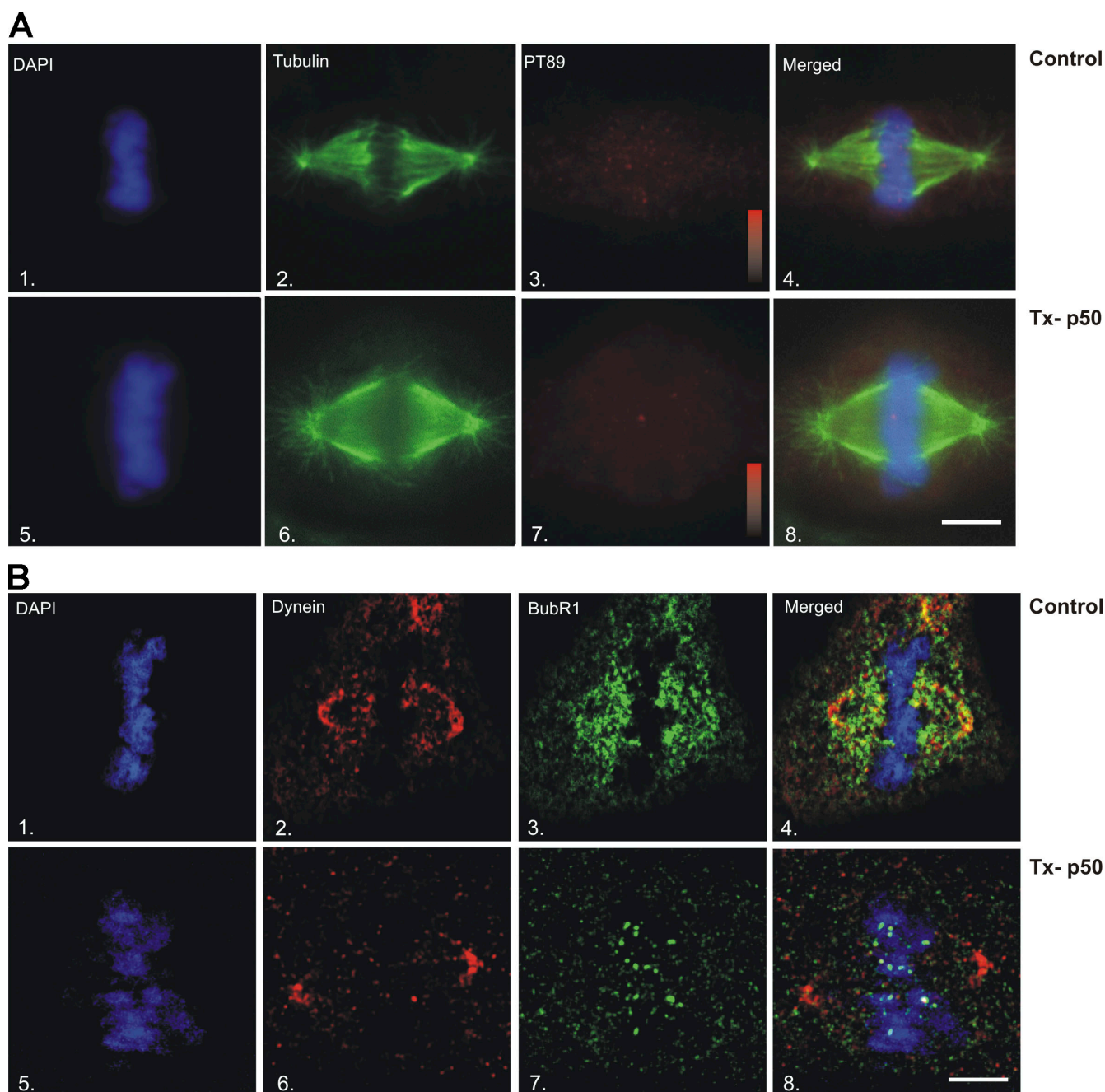
Figure 8. **Impact of p50(dynamitin) expression on dynein-mediated streaming.** (A) A comparison of control (1–4) and p50(dynamitin)-transfected (Tx-p50) cells (5–8) reveals loss of PT89 labeling (3 and 7) at metaphase after p50(dynamitin) expression. Intensity scales in panels 3 and 7 represent signal intensities of 0–800 intensity units in matched experiments. (B) Formaldehyde-fixed NRK2 cells stained for BubR1 and total dynein. Comparing control (1–4) and p50(dynamitin)-transfected cells (5–8), total dynein (2 and 6) shifts from kinetochores to kinetochore fibers and poles by the time of chromosome alignment. In controls, BubR1 also shifts from kinetochore labeling to broad labeling of the spindle fibers (3 and 4). In contrast, BubR1 remains on kinetochores after chromosome alignment in p50(dynamitin)-expressing cells (7 and 8) despite the shift in dynein. Bars, 5 µm.

with the dynein cofactor dynactin, thereby allowing poleward movement of kinetochore components in a process known as streaming. Because poleward streaming is the basis of checkpoint protein removal at metaphase, this work suggests that kinetochore dynein is a central component of the SAC.

Mitotic phosphorylation of dynein subunits

Several experiments support mitotic phosphorylation of dynein subunits. Mitotic phosphorylation of the light ICs (LICs) was

identified in CSF-arrested *Xenopus* egg extracts (Niclas et al., 1996). Although *cdc2* has been implicated in this phosphorylation (Dell et al., 2000), LIC phosphorylation at one *cdc2* consensus site was the same in both mitotic and interphase extracts (Addinall et al., 2001). A mitotic gel shift of the LICs was not detected in the synchronized HeLa extracts but will require further analysis.

One previous study identified the dynein ICs as a mitotic phosphorylation substrate. Huang et al. (1999) demonstrated IC

phosphorylation in CSF-arrested *Xenopus* egg extracts and a mitotic gel shift suggestive of phosphorylation in HeLa extracts. Although the phosphorylation sites were not mapped in previous work, these findings are consistent with our analysis of mitotic dynein ICs.

Phosphorylation and dynein localization

An interesting implication of this work is that dynein exists in two different states at kinetochores and is anchored by distinct binding partners. Previous models assumed a homogeneous population of dynein at kinetochores. Dynactin depletion appears to primarily affect the dephospho form of dynein. Given the gradual conversion of PT89-dynein to dephosphodynein during chromosome alignment, the impact of dynactin depletion would be variable. The effect of dynactin depletion on total dynein also suggests that dephosphodynein resides at kinetochores for some period of time before translocating to spindle poles.

The identification of *zw10* as a binding partner for phosphodynein is also consistent with previous work. Because *zw10* binds phosphodynein directly (this study) and dephosphodynein indirectly (via dynactin; Starr et al., 1998), loss of *zw10* should have a dramatic impact on total dynein levels at kinetochores. siRNA-driven depletion of *zw10* was more effective at reducing dynein levels than p50(dynamitin) expression (Kops et al., 2005).

Defects induced by p50(dynamitin) expression

Our analysis of cells expressing different levels of p50(dynamitin) suggests a dosage effect. Transfected p50(dynamitin) can function as a kinetochore marker without disrupting spindle function if expressed at very low levels. When expressed at high levels, p50(dynamitin) induces global problems with dynactin at spindle poles, the cell cortex, and kinetochores (Echeverri et al., 1996). At levels of expression between these extremes, p50(dynamitin) affects kinetochore dynactin localization without affecting other dynactin populations. This could reflect the role of p50(dynamitin) in targeting dynactin to kinetochores through an interaction with *zw10* (Starr et al., 1998). It could also reflect the cumulative effects of excess p50(dynamitin) on dynactin assembly and stability (Melkonian et al., 2007).

Changes in dynein localization during chromosome alignment

Although the ability of a single unaligned chromosome to block anaphase onset is one of the most intriguing aspects of the SAC, the mechanisms that allow an individual chromosome to assess its alignment are incompletely understood. An intriguing aspect of this new model is the autonomous nature of dynein function. Based on electron microscopy of individual kinetochores, it is likely that each kinetochore contains tens of MTs and many dynein molecules per MT (Rieder, 1982; McEwen et al., 1998). In the absence of MT attachment, this model predicts that kinetochores recruit PT89-dynein but fail to stimulate dynein dephosphorylation. These kinetochores retain phosphodynein and the ability to generate activated anaphase inhibitors.

This would be similar to recent work in which the ability of dynein to mediate "self-removal" was disrupted (Varma et al., 2008). The inability of dynein to produce poleward motility induced metaphase arrest/delay. However, kinetochores under tension at metaphase stimulate maximal dynein dephosphorylation. These kinetochores release dynein and checkpoint proteins quickly by streaming, thereby undermining the normal checkpoint activation process (Howell et al., 2001; for review see Musacchio and Salmon, 2007). Perhaps more ambiguous are the stages in between these extremes. PT89-dynein labeling indicates a gradual shift in dynein dephosphorylation that reflects progress in alignment. Presumably the changes in labeling correlate with the percentage of dyneins undergoing dephosphorylation. If true, this would suggest that interactions between MTs and kinetochores are sufficient for some dynein dephosphorylation throughout prometaphase. However, the efficiency of this process improves as chromosomes approach the metaphase plate.

Tension versus attachment

One implication of this study is that dynein dephosphorylation begins at bioriented MT attachment and increases gradually until metaphase alignment. This is based on the changes in PT89 signal that accompany progression through prometaphase. As a result, dynein-based streaming is not likely to begin precisely at alignment but rather increase gradually from spindle association to metaphase. In this model, the relative contributions of MT attachment and tension could be confusing because they represent the extremes in a gradual process. Given the poor preservation of chromosome oscillations by fixed cell analysis, it is challenging to assess transient changes in tension during prometaphase. Additional live cell analysis will improve our understanding of tension-activated changes during mitosis.
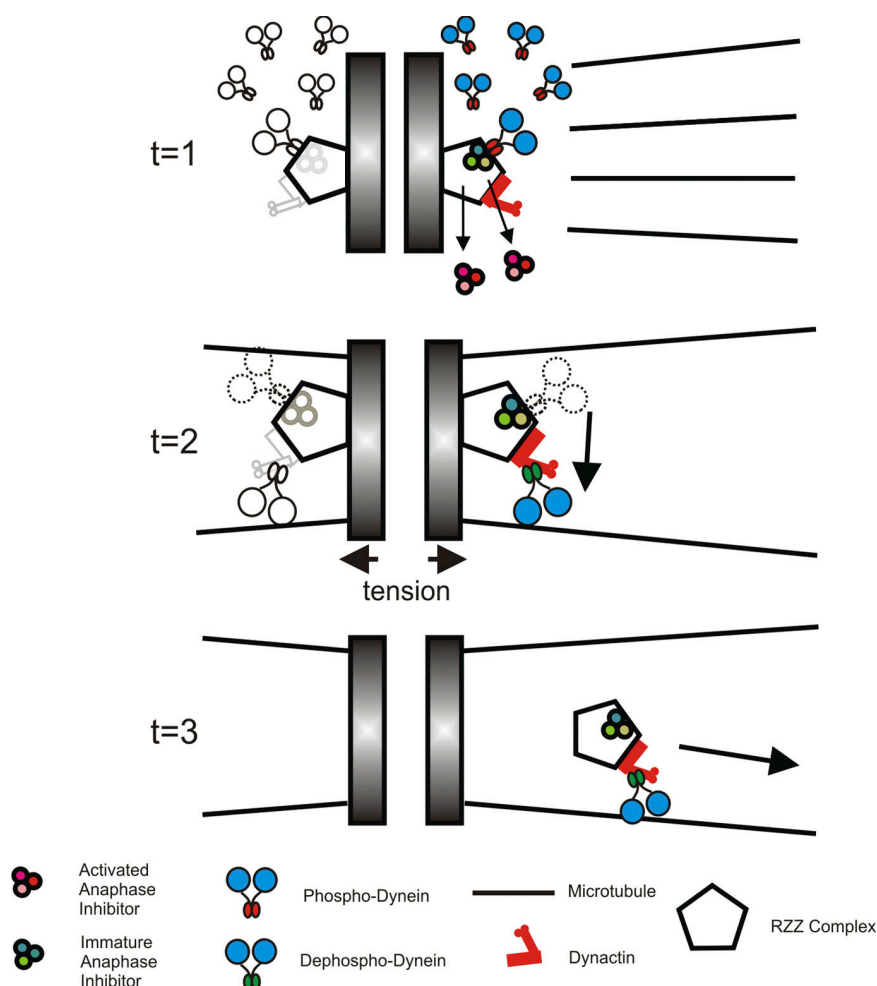
Identification of a dynein phosphatase

Based on phosphatase inhibition experiments, PP1-γ is implicated in activating dynein streaming. Inhibition of PP1-γ induced accumulation of phosphodynein at kinetochores (Fig. 6) and led to defects in the checkpoint silencing at metaphase. Although phosphatase inhibitors could act directly or indirectly through other enzymes, the localization of PP1-γ to kinetochores (Trinkle-Mulcahy et al., 2003) as well as the impact of phosphatase-dead mutant PP1-γ transfection (Lesage et al., 2004) suggest a direct role in dynein dephosphorylation. The activity of the dynein phosphatase appears to increase during chromosome alignment despite the presence of PP1-γ on kinetochores throughout prometaphase (Trinkle-Mulcahy et al., 2003). This suggests that dynein dephosphorylation reflects the progress in chromosome alignment. Other substrates for PP1-γ could play important roles in the checkpoint as well, and it will be important to identify these candidates.

A new model for dynein activity in the SAC

This work provides a new model for dynein kinetics at kinetochores. Dynein is recruited to kinetochores as a phosphoprotein and remains in this state until MT attachment (Fig. 9, t = 1). This is the state observed after MT depolymerization; however, one could

Figure 9. New model for regulation of cytoplasmic dynein at kinetochores. During prometaphase, dynein is loaded onto kinetochores via binding of phosphodynein to *zw10* (t = 1). As MTs attach to kinetochores and chromosomes congress to the metaphase plate (t = 2), dynein undergoes dephosphorylation, shifting binding from *zw10* to dynactin (t = 2). This transition stimulates dynein for translocation away from kinetochores (t = 3). Because activated dynein contributes to the removal of anaphase inhibitors from kinetochores, dynein dephosphorylation reduces the ability of kinetochores to produce active anaphase inhibitors.

predict that this is the basis of recruitment throughout prometaphase. Once kinetochores acquire bioriented MT attachment, some fraction of dyneins undergo dephosphorylation and translocate to spindle poles (Fig. 9, t = 2). These dyneins transport a fraction of checkpoint proteins away from kinetochores, thereby reducing the overall production of anaphase inhibitors. Early in prometaphase when dynein dephosphorylation is a low frequency event, translocating dynein represents a minor population, and sufficient levels of anaphase inhibition are maintained. As chromosomes reach the metaphase plate and complete the late stages of alignment, however, dynein dephosphorylation becomes very efficient, and the translocating population of dynein becomes dominant (Fig. 9, t = 3). The dynein depletion that ensues leads to diminished activation of anaphase inhibitors and anaphase onset. As a result, the gradual activation of dynein dephosphorylation that accompanies MT attachment and chromosome movement provides a new mechanism to couple chromosome alignment with anaphase onset.

Materials and methods

Dynein purification and analysis
Synchronized HeLa cells were prepared as described previously (Merrill, 1998). Cytoplasmic dynein was isolated by immunoprecipitation using the 74.1 antibody (Dillman and Pfister, 1994) and protein A–Sepharose beads (GE Healthcare). SDS-PAGE and λ-phosphatase (New England Biolabs, Inc.) treatment were performed using standard methods. Gel bands containing

the shifted IC polypeptide were subjected to proteolytic digestion, capillary HPLC (Waters), and tandem MS analysis using a Deca XP Plus (Thermo-Finnigan) in the Harvard University Microchemistry and Proteomics Facility.

Antibodies and immunological techniques
A rabbit polyclonal antibody was generated by standard methods against a synthetic peptide spanning aa 81–97 of IC-2C (SPSSKSVS**T**PSEAGSQD) and containing a phosphorylated threonine at position T89 (Open Biosystems). The bold letter indicates the phosphorylated residue. Immunofluorescence microscopy (IFM) assays were performed on methanol/formaldehyde-fixed cells with rabbit sera or monoclonal antibodies and Cy2-, Cy3-, or Cy5-conjugated secondary antibodies (Jackson ImmunoResearch Laboratories). DNA was detected using DAPI, total dynein with 74.1 (Dillman and Pfister, 1994) or V3 (Vaughan et al., 2001), kinetochores with antibodies against ACA (Antibodies, Inc.) or BubR1 (BD), and tubulin with DM1A (Antibodies, Inc.). p150^{Glued} was detected with a rabbit polyclonal antibody (Vaughan et al., 1999). *zw10* was immunoprecipitated with monoclonal antibodies (Chan et al., 2000). Immunoprecipitations were performed with antidynein or anti-*zw10* antibodies and protein A–Sepharose beads.

Blot overlay assays
Blot overlay assays were performed as described previously (Vaughan and Vallee, 1995) using a recombinant p150^{Glued} fragment spanning residues 1–811 or IC-2C fragments spanning residues 1–284. Binding results after electrochemiluminescence detection were recorded on autoradiographic film and digitized using a Fluorchem 8900 (Alpha Innotec). Signal intensity was summed in the area of the bands, and the intensity of film background was subtracted. For each of three experiments, the signal of the interphase sample was scored as 100%, and the signal of the mitotic sample was assessed as a percentage of the interphase sample. The mean of each dataset was plotted with SD.

DNA constructs and transfections
Mammalian expression constructs encoding truncated IC-2C (Vaughan et al., 2001), mCherry-tagged p50(dynamitin) (Echeverri et al., 1996), and PP1-γ

(L. Trinkle-Mulcahy, University of Dundee, Dundee, Scotland, UK; Trinkle-Mulcahy et al., 2003; Lesage et al., 2004) were prepared using standard techniques and confirmed by DNA sequencing. shRNA constructs against rat *zw10* (5′-TCACCCAGGTGGACACTCTAT-3′ and 5′-GAGGACATCTCGACT-GAAGAT-3′) were obtained from Superarray, Inc. An shRNA construct against p150^{Glued} was designed based on the rat p150^{Glued} sequence (5′-CACATGC-TAACTTCTTGA-3′). Plasmids were transfected into NRK2 cells using nucleo-poration (Amaxa, Inc.). Existing antibodies against *zw10* and p150^{Glued} were used to confirm protein depletion by Western blot analysis of the extracts.

Cell culture and treatments
NRK2 cells (Fishkind and Wang, 1993) were treated with 5 µM nocodazole (Invitrogen) for 3 h to depolymerize MTs, with 10 µM taxol (Sigma-Aldrich) for 30 min to reduce tension at kinetochores (Waters et al., 1998), or with 200 pM calyculin A (EMD) for 2 h to inhibit PP1 and PP2 phosphatases. Interkineto-chore distance measurements were obtained from individual planes of decon-volved z series of mitotic cells and assessed from a pool of 10 cells each. Peak-to-peak distance measurements were collected from kinetochores labeled with anti-ACA antibodies.

IFM and live cell imaging
Images were acquired on a microscope (Axiovert 200MOT; Carl Zeiss, Inc.) operated with Metamorph software (MDS Analytical Technologies) and a camera (CoolSNAP HQ; Roper Scientific). Images were collected at room temperature (fixed cell) or 37°C (live cell) using a 63× NA 1.4 objective. Data were collected as z series and subjected to digital deconvolution with Meta-morph. Because of the signal complexity, individual representative planes are presented in figures. Using matched illumination, exposure times, and anti-body conditions, raw image intensities were used to determine intensity scales for each experiment. These raw data were maintained through image pro-cessing in Photoshop (Adobe Software, Inc.) and Coreldraw (Corel) and pre-sented in a pseudocolor scale to convey relative image intensities. For live cell imaging experiments, time-lapse image sequences were collected on a similar microscope fit with a camera (Cascade 1k; Roper Scientific). Scales are pre-sented in the figure legends.

Statistical analysis
Statistical analysis of intensity measurements, interkinetochore distance mea-surements, signal ratios, and protein–protein interaction assays was per-formed in Excel (Microsoft). P-values of comparisons between control and experimental measurements were determined with a two-tailed t test assuming unequal variance. Confidence levels were chosen at $P \leq 0.05$.

Online supplemental material
Fig. S1 shows tandem MS analysis and biochemical characterization of T89 mutants. Fig. S2 shows characterization of PT89 antibody by IFM, Western blotting and immunoprecipitation, and sensitivity to in vitro phosphoryla-tion by p38-MAPK. Fig. S3 shows the detection of transfected dynein IC constructs by PT89 antibody. Fig. S4 shows statistical analysis of PT89 in-tensities relative to kinetochore proteins, timing of mitotic progression, and interkinetochore distance measurements. Video 1 shows the mitotic timing of an NRK2 cell expressing GFP-H2B. Video 2 shows the mitotic timing of an NRK2 cell coexpressing GFP-H2B and mCherry-p50(dynamitin). Video 3 shows the streaming of GFP-p50(dynamitin) from kinetochores in a control NRK2 cell. Video 4 shows the loss of streaming in an NRK2 cell expressing GFP-p50(dynamitin) after taxol treatment. Online supplemental material is available at http://www.jcb.org/cgi/content/full/jcb.200804114/DC1.

References

Adames, N.R., and J.A. Cooper. 2000. Microtubule interactions with the cell cor-tex causing nuclear movements in *Saccharomyces cerevisiae*. *J. Cell Biol.* 149:863–874.

Addinall, S.G., P.S. Mayr, S. Doyle, J.K. Sheehan, P.G. Woodman, and V.J. Allan. 2001. Phosphorylation by cdc2-CyclinB1 kinase releases cytoplas-mic dynein from membranes. *J. Biol. Chem.* 276:15939–15944.

Banks, J.D., and R. Heald. 2001. Chromosome movement: dynein-out at the ki-netochore. *Curr. Biol.* 11:R128–R131.

Basto, R., F. Scaerou, S. Mische, E. Wojcik, C. Lefebvre, R. Gomes, T. Hays, and R. Karess. 2004. In vivo dynamics of the rough deal checkpoint protein during *Drosophila* mitosis. *Curr. Biol.* 14:56–61.

Cande, W.Z., and S.M. Wolniak. 1978. Chromosome movement in lysed mitotic cells is inhibited by vanadate. *J. Cell Biol.* 79:573–580.

Carminati, J.L., and T. Stearns. 1997. Microtubules orient the mitotic spindle in yeast through dynein-dependent interactions with the cell cortex. *J. Cell Biol.* 138:629–641.

Chan, G.K., S.A. Jablonski, D.A. Starr, M.L. Goldberg, and T.J. Yen. 2000. Human zw10 and ROD are mitotic checkpoint proteins that bind to ki-netochores. *Nat. Cell Biol.* 2:944–947.

Deacon, S.W., A.S. Serpinskaya, P.S. Vaughan, M. Lopez Fanarraga, I. Vernos, K.T. Vaughan, and V.I. Gelfand. 2003. Dynactin is required for bidirec-tional organelle transport. *J. Cell Biol.* 160:297–301.

Dell, K.R., C.W. Turck, and R.D. Vale. 2000. Mitotic phosphorylation of the dy-nein light intermediate chain is mediated by cdc2 kinase. *Traffic.* 1:38–44.

Dillman, J.F. III, and K.K. Pfister. 1994. Differential phosphorylation in vivo of cytoplasmic dynein associated with anterogradely moving organelles. *J. Cell Biol.* 127:1671–1681.

Dillman, J.F. III, L.P. Dabney, S. Karki, B.M. Paschal, E.L.F. Holzbaur, and K.K. Pfister. 1996. Functional analysis of dynactin and cytoplasmic dynein in slow axonal transport. *J. Neurosci.* 16:6742–6752.

Dujardin, D.L., and R.B. Vallee. 2002. Dynein at the cortex. *Curr. Opin. Cell Biol.* 14:44–49.

Echeverri, C.J., B.M. Paschal, K.T. Vaughan, and R.B. Vallee. 1996. Molecular characterization of the 50-kD subunit of dynactin reveals function for the complex in chromosome alignment and spindle organization during mi-tosis. *J. Cell Biol.* 132:617–633.

Faulkner, N.E., D.L. Dujardin, C.Y. Tai, K.T. Vaughan, C.B. O'Connell, Y. Wang, and R.B. Vallee. 2000. A role for the lissencephaly gene LIS-1 in mitosis and cytoplasmic dynein function. *Nat. Cell Biol.* 2:784–791.

Fishkind, D.J., and Y.L. Wang. 1993. Orientation and three-dimensional or-ganization of actin filaments in dividing cultured cells. *J. Cell Biol.* 123:837–848.

Gaglio, T., A. Saredi, J.B. Bingham, J. Hasbani, S.R. Gill, T.A. Schroer, and D.A. Compton. 1996. Opposing motor activities are required for the organiza-tion of the mammalian mitotic spindle pole. *J. Cell Biol.* 135:399–414.

Gorbsky, G.J., and W.A. Ricketts. 1993. Differential expression of a phos-phoepitope at the kinetochores of moving chromosomes. *J. Cell Biol.* 122:1311–1321.

Griffis, E.R., N. Stuurman, and R.D. Vale. 2007. Spindly, a novel protein essen-tial for silencing the spindle assembly checkpoint, recruits dynein to the kinetochore. *J. Cell Biol.* 177:1005–1015.

Heald, R., R. Tournebize, T. Blank, R. Sandaltzopoulos, P. Becker, A. Hyman, and E. Karsenti. 1996. Self-organization of microtubules into bipolar spindles around artificial chromosomes in *Xenopus* egg extracts. *Nature.* 382:420–425.

Hoffman, D.B., C.G. Pearson, T.J. Yen, B.J. Howell, and E.D. Salmon. 2001. Microtubule-dependent changes in assembly of microtubule motor pro-teins and mitotic spindle checkpoint proteins at PtK1 kinetochores. *Mol. Biol. Cell.* 12:1995–2009.

Howell, B.J., D.B. Hoffman, G. Fang, A.W. Murray, and E.D. Salmon. 2000. Visualization of Mad2 dynamics at kinetochores, along spindle fibers, and at spindle poles in living cells. *J. Cell Biol.* 150:1233–1250.

Howell, B.J., B.F. McEwen, J.C. Canman, D.B. Hoffman, E.M. Farrar, C.L. Rieder, and E.D. Salmon. 2001. Cytoplasmic dynein/dynactin drives ki-netochore protein transport to the spindle poles and has a role in mitotic spindle checkpoint inactivation. *J. Cell Biol.* 155:1159–1172.

Huang, C.Y., C.P. Chang, C.L. Huang, and J.E. Ferrell Jr. 1999. M phase phos-phorylation of cytoplasmic dynein intermediate chain and p150(Glued). *J. Biol. Chem.* 274:14262–14269.

Karess, R. 2005. Rod-zw10-zwilch: a key player in the spindle checkpoint. *Trends Cell Biol.* 15:386–392.

King, J.M., T.S. Hays, and R.B. Nicklas. 2000. Dynein is a transient kinetochore component whose binding is regulated by microtubule attachment, not tension. *J. Cell Biol.* 151:739–748.

Kops, G.J., Y. Kim, B.A. Weaver, Y. Mao, I. McLeod, J.R. Yates III, M. Tagaya, and D.W. Cleveland. 2005. ZW10 links mitotic checkpoint signaling to the structural kinetochore. *J. Cell Biol.* 169:49–60.

Lesage, B., M. Beullens, M. Nuytten, A. Van Eynde, S. Keppens, B. Himpens, and M. Bollen. 2004. Interactor-mediated nuclear translocation and reten-tion of protein phosphatase-1. *J. Biol. Chem.* 279:55978–55984.

Li, Y.Y., E. Yeh, T. Hays, and K. Bloom. 1993. Disruption of mitotic spindle orientation in a yeast dynein mutant. *Proc. Natl. Acad. Sci. USA.* 90:10096–10100.

Lo, K.W., S. Naisbitt, J.S. Fan, M. Sheng, and M. Zhang. 2001. The 8-kDa dynein light chain binds to its targets via a conserved (K/R)XTQT motif. *J. Biol. Chem.* 276:14059–14066.

McEwen, B.F., C.E. Hsieh, A.L. Mattheyses, and C.L. Rieder. 1998. A new look at kinetochore structure in vertebrate somatic cells using high-pressure freezing and freeze substitution. *Chromosoma.* 107:366–375.

McIntosh, J.R., E.L. Grishchuk, and R.R. West. 2002. Chromosome-microtubule interactions during mitosis. *Annu. Rev. Cell Dev. Biol.* 18:193–219.

Melkonian, K.A., K.C. Maier, J.E. Godfrey, M. Rodgers, and T.A. Schroer. 2007. Mechanism of dynamitin-mediated disruption of dynactin. *J. Biol. Chem.* 282:19355–19364.

Merdes, A., R. Heald, K. Samejima, W.C. Earnshaw, and D.W. Cleveland. 2000. Formation of spindle poles by dynein/dynactin-dependent transport of NuMA. *J. Cell Biol.* 149:851–862.

Merrill, G.F. 1998. Cell synchronization. *Methods Cell Biol.* 57:229–249.

Mok, Y.K., K.W. Lo, and M. Zhang. 2001. Structure of Tctex-1 and its interaction with cytoplasmic dynein intermediate chain. *J. Biol. Chem.* 276:14067–14074.

Muhua, L., T.S. Karpova, and J.A. Cooper. 1994. A yeast actin-related protein homologous to that in vertebrate dynactin complex is important for spindle orientation and nuclear migration. *Cell.* 78:669–679.

Musacchio, A., and E.D. Salmon. 2007. The spindle-assembly checkpoint in space and time. *Nat. Rev. Mol. Cell Biol.* 8:379–393.

Nicklas, R.B., S.C. Ward, and G.J. Gorbsky. 1995. Kinetochore chemistry is sensitive to tension and may link mitotic forces to a cell cycle checkpoint. *J. Cell Biol.* 130:929–939.

Niclas, J., V.J. Allan, and R.D. Vale. 1996. Cell cycle regulation of dynein association with membranes modulates microtubule-based organelle transport. *J. Cell Biol.* 133:585–593.

O'Connell, C.B., and Y.L. Wang. 2000. Mammalian spindle orientation and position respond to changes in cell shape in a dynein-dependent fashion. *Mol. Biol. Cell.* 11:1765–1774.

Pfarr, C.M., M. Coue, P.M. Grissom, T.S. Hays, M.E. Porter, and J.R. McIntosh. 1990. Cytoplasmic dynein is localized to kinetochores during mitosis. *Nature.* 345:263–265.

Pinsky, B.A., and S. Biggins. 2005. The spindle checkpoint: tension versus attachment. *Trends Cell Biol.* 15:486–493.

Rieder, C.L. 1982. The formation, structure, and composition of the mammalian kinetochore and kinetochore fiber. *Int. Rev. Cytol.* 79:1–58.

Rieder, C.L., and S.P. Alexander. 1990. Kinetochores are transported poleward along a single astral microtubule during chromosome attachment to the spindle in newt lung cells. *J. Cell Biol.* 110:81–95.

Rusan, N.M., U.S. Tulu, C. Fagerstrom, and P. Wadsworth. 2002. Reorganization of the microtubule array in prophase/prometaphase requires cytoplasmic dynein-dependent microtubule transport. *J. Cell Biol.* 158:997–1003.

Savoian, M.S., M.L. Goldberg, and C.L. Rieder. 2000. The rate of poleward chromosome motion is attenuated in *Drosophila zw10* and *rod* mutants. *Nat. Cell Biol.* 2:948–952.

Shannon, K.B., J.C. Canman, and E.D. Salmon. 2002. Mad2 and BubR1 function in a single checkpoint pathway that responds to a loss of tension. *Mol. Biol. Cell.* 13:3706–3719.

Sharp, D.J., G.C. Rogers, and J.M. Scholey. 2000. Cytoplasmic dynein is required for poleward chromosome movement during mitosis in *Drosophila* embryos. *Nat. Cell Biol.* 2:922–930.

Starr, D.A., B.C. Williams, T.S. Hays, and M.L. Goldberg. 1998. ZW10 helps recruit dynactin and dynein to the kinetochore. *J. Cell Biol.* 142:763–774.

Stehman, S.A., Y. Chen, R.J. McKenney, and R.B. Vallee. 2007. NudE and NudEL are required for mitotic progression and are involved in dynein recruitment to kinetochores. *J. Cell Biol.* 178:583–594.

Steuer, E.R., L. Wordeman, T.A. Schroer, and M.P. Sheetz. 1990. Localization of cytoplasmic dynein to mitotic spindles and kinetochores. *Nature.* 345:266–268.

Susalka, S.J., K. Nikulina, M.W. Salata, P.S. Vaughan, S.M. King, K.T. Vaughan, and K.K. Pfister. 2002. The roadblock light chain binds a novel region of the cytoplasmic dynein intermediate chain. *J. Biol. Chem.* 277:32939–32946.

Trinkle-Mulcahy, L., P.D. Andrews, S. Wickramasinghe, J. Sleeman, A. Prescott, Y.W. Lam, C. Lyon, J.R. Swedlow, and A.I. Lamond. 2003. Time-lapse imaging reveals dynamic relocalization of PP1gamma throughout the mammalian cell cycle. *Mol. Biol. Cell.* 14:107–117.

Vaisberg, E.A., M.P. Koonce, and J.R. McIntosh. 1993. Cytoplasmic dynein plays a role in mammalian mitotic spindle formation. *J. Cell Biol.* 123:849–858.

Varma, D., P. Monzo, S.A. Stehman, and R.B. Vallee. 2008. Direct role of dynein motor in stable kinetochore-microtubule attachment, orientation, and alignment. *J. Cell Biol.* 182:1045–1054.

Vaughan, K.T., and R.B. Vallee. 1995. Cytoplasmic dynein binds dynactin through a direct interaction between the intermediate chains and p150 [Glued]. *J. Cell Biol.* 131:1507–1516.

Vaughan, K.T., S.H. Hughes, C.J. Echeverri, N.F. Faulkner, and R.B. Vallee. 1999. Co-localization of dynactin and cytoplasmic dynein with CLIP-170 at microtubules distal ends. *J. Cell Sci.* 112:1437–1447.

Vaughan, P.S., J.D. Leszyk, and K.T. Vaughan. 2001. Cytoplasmic dynein intermediate chain phosphorylation regulates binding to dynactin. *J. Biol. Chem.* 276:26171–26179.

Vergnolle, M.A., and S.S. Taylor. 2007. Cenp-F links kinetochores to Ndel1/Nde1/Lis1/dynein microtubule motor complexes. *Curr. Biol.* 17:1173–1179.

Waters, J.C., R. Chen, A.W. Murray, and E.D. Salmon. 1998. Localization of Mad2 to kinetochores depends on microtubule attachment, not tension. *J. Cell Biol.* 141:1181–1191.

Wilkerson, C.G., S.M. King, A. Koutoulis, G.J. Pazour, and G.B. Witman. 1995. The 78,000 M_r intermediate chain of *Chlamydomonas* outer arm dynein is a WD-repeat protein required for arm assembly. *J. Cell Biol.* 129:169–178.

Williams, B.C., Z. Li, S. Liu, E.V. Williams, G. Leung, T.J. Yen, and M.L. Goldberg. 2003. Zwilch, a new component of the ZW10/ROD complex required for kinetochore functions. *Mol. Biol. Cell.* 14:1379–1391.

Wojcik, E., R. Basto, M. Serr, F. Scaerou, R. Karess, and T. Hays. 2001. Kinetochore dynein: its dynamics and role in the transport of the Rough deal checkpoint protein. *Nat. Cell Biol.* 3:1001–1007.

Wordeman, L., E.R. Steuer, M.P. Sheetz, and T. Mitchison. 1991. Chemical subdomains within the kinetochore domain of isolated CHO mitotic chromosomes. *J. Cell Biol.* 114:285–294.

Yang, Z., U.S. Tulu, P. Wadsworth, and C.L. Rieder. 2007. Kinetochore dynein is required for chromosome motion and congression independent of the spindle checkpoint. *Curr. Biol.* 17:973–980.

Zhou, T., W. Zimmerman, X. Liu, and R.L. Erikson. 2006. A mammalian NudC-like protein essential for dynein stability and cell viability. *Proc. Natl. Acad. Sci. USA.* 103:9039–9044.